The 'tumour suppressor' or 'anti-oncogene'[2] bears an intriguing relationship to the erbA phenotype described here. The inactivation or loss of both copies of these genes has been genetically implicated in a number of human tumours[2,30]. Thus, it is the absence of the product that leads to transformation in some cell types and in these cases tumour development requires at least two genetic changes. The experiments in this study suggest that v-erbA contributes to cellular transformation by inhibiting the function of its normal endogenous counterpart. We propose that in some cases, loss of function resulting from a single mutation would be sufficient as a causal event in tumorigenesis for some recessive oncogenes. Therefore, the dominant negative phenotype may be a prototype of a new and more general mechanism of cellular transformation. □

Received 8 March; accepted 15 May 1989.

1. Bishop, J. M. *Science* **235,** 305–311 (1987).
2. Klein, G. A. *Science* **238,** 1539–1545 (1987).
3. Land, H., Parada, L. F. & Weinberg, R. A. *Science* **222,** 771–778 (1983).
4. Damm, K., Beug, H., Graf, T. & Vennström, B. *EMBO J.* **6,** 375–382 (1987).
5. Kahn, P. *et al. Cell* **45,** 349–356 (1986).
6. Frykberg, L. *et al. Cell* **32,** 227–238 (1983).
7. Zenke, M. *et al. Cell* **52,** 107–119 (1988).
8. Sap, J. *et al. Nature* **324,** 635–640 (1986).
9. Weinberger, C. *et al. Nature* **324,** 641–646 (1986).
10. Evans, R. M. *Science* **240,** 889–895 (1988).
11. Thompson, C. C. & Evans, R. M. *Proc. natn. Acad. Sci. U.S.A.* **86,** 3494–3498 (1989).
12. Hollenberg, S. M., Giguère, V., Segui, P. & Evans, R. M. *Cell* **49,** 39–46 (1987).
13. Hollenberg, S. M. & Evans, R. M. *Cell* **55,** 899–906 (1988).
14. Godowski, P. J., Rusconi, S., Miesfeld, R. & Yamamoto, K. R. *Nature* **325,** 365–368 (1987).
15. Kumar, V. *et al. Cell* **51,** 941–951 (1987).
16. Adler, S., Waterman, M. L., He, X. & Rosenfeld, M. G. *Cell* **52,** 685–695 (1988).
17. Carson, M. A. *et al. Mol. Endo.* **1,** 791–801 (1987).
18. Gronemeyer, H. *et al. EMBO J.* **6,** 3985–3994 (1987).
19. Muñoz, A. *et al. EMBO J.* **7,** 155–159 (1988).
20. Thompson, C. C., Weinberger, C., Lebo, R. & Evans, R. M. *Science* **237,** 1610–1614 (1987).
21. Glass, C. K. *et al. Nature* **329,** 738–741 (1987).
22. Glass, C. K., Holloway, J. M., Devary, O. V. & Rosenfeld, M. G. *Cell* **54,** 313–323 (1988).
23. Luckow, B & Schütz, G. *Nucleic Acids Res.* **15,** 5490 (1987).
24. Vennström, B., Fanshier, L., Moscovici, C. & Bishop, J. M. *J. Virol.* **36,** 575–585 (1980).
25. Herskowitz, I. *Nature,* **329,** 219–222 (1987).
26. Lavin, T. N., Baxter, J. D. & Horita, S. *J. biol. Chem.* **263,** 9418–9426 (1988).
27. Schüle, R., Muller, M., Kaltschmidt, C. & Renkawitz, R. *Science* **242,** 1418–1420 (1988).
28. Strähle, U., Schmid, W. & Schütz, G. *EMBO J.* **7,** 3389–3395 (1988).
29. Koenig, R. J. *et al. Nature* **337,** 659–661 (1989).
30. Friend, S. H. *et al. Nature* **323,** 643–646 (1986).
31. Giguère, V., Ong, E. S., Segui, P. & Evans, R. M. *Nature* **330,** 624–629 (1987).
32. Samuels, H. H., Stanley, F. & Casanova, J. *Endocrinology* **105,** 80–85 (1979).
33. Herbomel, P., Bourachot, B. & Yaniv, M. *Cell* **39,** 653–662 (1984).
34. Gorman, C. M., Moffat, L. F. & Howard, B. H. *Molec. cell. Biol.* **2,** 1044–1051 (1982).
35. Giguère, V., Hollenberg, S. M., Rosenfeld, M. G. & Evans, R. M. *Cell* **46,** 645–652 (1986).
36. Kumar, V & Chambon, P. *Cell* **55,** 145–156 (1988).

ACKNOWLEDGEMENTS. We thank Drs Tony Hunter, Inder Verma, Jeff Arriza, Stan Hollenberg and Kazuhiko Umesono for advice on the manuscript, members of the Evans laboratory for discussions and Gail Cerelli for expert technical assistance. We also thank Dr Jeff Arriza for providing us with the plasmid hGR_{NX}, Drs Chris Glass and Geoff Rosenfeld for GH293TK and Drs Bruno Luckow and Günther Schütz for pBLCAT2. K.D. is the recipient of a postdoctoral fellowship from the Deutscher Akademischer Austauschdienst, Sonderprogramm Gentechnologie. C.C.T. is a predoctoral trainee in the Department of Biology, University of California, San Diego. R.M.E. is an investigator of the Howard Hughes Medical Institute. This work was supported by the Howard Hughes Medical Institute, the NIH and the Mathers Foundation.

Structural parts involved in activation and inactivation of the sodium channel

Walter Stühmer*, Franco Conti†, Harukazu Suzuki*‡ & Xiaodong Wang*
Masaharu Noda§, Naoki Yahagi§, Hideo Kubo§ & Shosaku Numa§

* Max-Planck-Institut für biophysikalische Chemie, D-3400 Göttingen, FRG
† Istituto di Cibernetica e Biofisica, CNR, I-16146 Genova, Italy
§ Departments of Medical Chemistry and Molecular Genetics, Kyoto University Faculty of Medicine, Kyoto 606, Japan

Structure–function relationships of the sodium channel expressed in *Xenopus* oocytes have been investigated by the combined use of site-directed mutagenesis and patch-clamp recording. This study provides evidence that the positive charges in segment S4 are involved in the voltage-sensing mechanism for activation of the channel and that the region between repeats III and IV is important for its inactivation.

THE voltage-gated sodium channel is essential for the generation of action potentials in many excitable cells[1,2]. Voltage-gated ionic channels must have charged structures that can move within the membrane and thus sense the membrane electric field. These movements produce a measurable current called the gating current[3,4], but the localization and identification of these structures within a channel protein are uncertain. The primary structures of the *Electrophorus* electroplax sodium channel[5] and of three distinct sodium channels from rat brain[6,7] have been elucidated by cloning and sequence analysis of the complementary DNAs. The partial amino-acid sequence of the sodium channel from *Drosophila* has also been deduced from the genomic DNA sequence[8]. The sodium channel is composed of about 2,000 amino-acid residues and contains four homologous internal repeats, each of which has six putative transmembrane segments. One of these segments, S4, contains several arginine or lysine residues at every third position with mostly nonpolar residues intervening between the basic residues. It has therefore been proposed that the positive charges in segment S4 serve as voltage sensor[5,6]. This hypothesis is supported by the fact that the unique structural features of segment S4 are shared by the slow calcium channel from rabbit skeletal muscle[9,10] and by potassium channels from *Drosophila*[11–13] and mammalian brain[14,15]. Functional sodium channels are expressed in *Xenopus* oocytes by microinjection of messenger RNAs derived from rat brain sodium channel cDNAs[16–19]. The sodium channels expressed from the cDNAs closely resemble those from native membranes in their properties, including the sensitivity to tetrodotoxin and saxitoxin, the rate at which the current turns on in response to a depolarizing voltage step (activation), the decay of the current during a maintained depolarization (inactivation) and the single-channel conductance.

To identify functional regions of the sodium channel, we have now investigated the effects of site-directed mutations of rat sodium channel II on its functional properties. First, to test the proposed role of segment S4 as voltage sensor, we have introduced point mutations into the S4 region so that positively charged amino-acid residues are replaced by neutral or negatively charged residues. A reduction in the net positive charge in segment S4 of repeat I leads to a decrease in the steepness of the potential dependence of activation, which provides experimental evidence for the direct involvement of the positive

‡ Permanent address: Departments of Medical Chemistry and Molecular Genetics, Kyoto University Faculty of Medicine, Kyoto 606, Japan

charges in this segment in the voltage-sensing device for activation. Second, to localize a region involved in inactivation, we have examined the effects of deletion or cleavage in putative cytoplasmic portions of the channel protein. Some of these mutants form functional sodium channels, two of which are characterized by inactivation rates much lower than that of the wild-type channel.

Construction of mutants

To facilitate the construction of mutant cDNAs, we prepared a recombinant plasmid, pRII-2A, which is a derivative of the plasmid pRII-2 (ref. 16) and carries the entire protein-coding sequence of the rat sodium channel II cDNA linked with the bacteriophage SP6 promoter. In pRII-2A, several unique restriction endonuclease sites have been introduced without altering the amino-acid sequence of sodium channel II (Fig. 1*a*). We confirmed that the messengerRNA derived from pRII-2A, when injected into *Xenopus* oocytes, yielded a sodium channel with functional properties indistinguishable from those of the sodium channel derived from pR11-2 (refs 16, 17). In the present investigation, pRII-2A was used to produce the mRNA specific for the wild-type sodium channel, and all plasmids carrying mutant cDNAs were constructed from pRII-2A. mRNAs synthesized by transcription *in vitro* of the cDNAs were injected into *Xenopus* oocytes and the resulting sodium channels were examined primarily by recording macroscopic sodium currents through cell-attached membrane patches of large diameter[17]. Current records were analysed according to the Hodgkin-Huxley (HH) equations[1] for the voltage dependence of the steady-state activation (m_∞) and inactivation (h_∞) parameters and of the respective time constants (τ_m and τ_h). The HH scheme, especially in that it treats m and h as independent parameters, does not provide a faithful interpretation of the actual set of structural transitions underlying the operation of sodium channels[20,21]. In the absence of any generally accepted more realistic scheme, however, the HH equations remain the most useful empirical framework for a fairly accurate description of the electrophysiological data with a minimum number of parameters.

Effects on activation

It is assumed that many of the positive charges in the putative voltage sensor segment S4 form ion pairs with negative charges in other transmembrane segments. The breakage of these ion

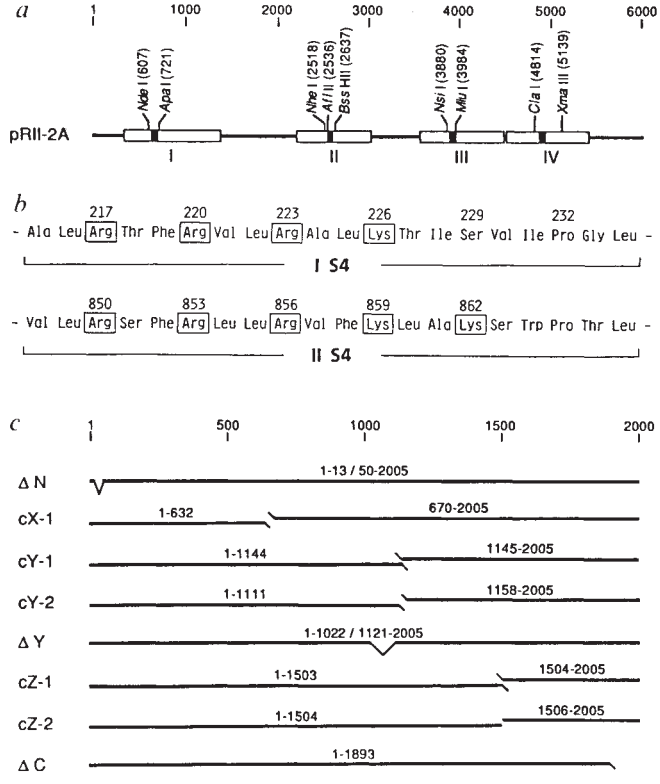

FIG. 1 Strategies for the construction of rat sodium channel II cDNA mutants. *a*, Restriction map of the recombinant plasmid pRII-2A used for site-directed mutagenesis. Only the protein-coding region is shown and nucleotide numbers[6] are given above the diagram. The coding regions for the four internal repeats (I–IV) are indicated by open boxes, and those for segment S4 in each repeat by filled boxes. The restriction endonuclease sites introduced are shown and identified by numbers (in parentheses) indicating the 5′-terminal nucleotide generated by cleavage. *b*, Amino-acid sequences[6] of segment S4 in repeat I (IS4) and repeat II (IIS4) of wild-type rat sodium channel II. The termini of the segments are tentatively assigned. Positively charged residues are boxed with solid lines and the numbers[6] of the relevant residues are given. *c*, Structures of deletion mutants and their combinations. The regions of rat sodium channel II carried by the individual mutants are shown by horizontal lines with the numbers of the constituent amino-acid residues; oblique lines at the termini of some constructs indicate the presence of short additional sequences (see text and Methods). V-shaped lines indicate internal deletions. Amino-acid numbers[6] are given above the diagram.

METHODS. The rat sodium channel II cDNA sequence in the plasmid pRII-2 (ref. 16) was modified by introducing unique restriction endonuclease sites into both sides of the coding region for each segment S4 to yield pRII-2A; the *Xba*I(541)/*Apa*I(721), *Dde*I(2498)/*Sph*I(2701), *Sau*3AI(3840)/*Ban*I(3995), *Fok*I(4793)/*Hha*I(4978) and *Sau*3AI(5112)/*Hpa*II(5142) segments were replaced by synthetic DNAs. pRII-2A differs from pRII-2 as follows (the substituted nucleotides with residue numbers[6] are given): A, 606, 2,520, 2,538, 2,539, 3,879, 4,812; G, 2,517, 2,540, 2,640, 3,987, 3,990, 4,815, 5,139; C, 2,518, 2,535, 2,637; T, 2,541, 3,988. Point mutations were introduced by replacing the *Nde*I(607)/*Apa*I(721) and/or the *Afl*II(2536)/*Bss*HII(2637) segment of pRII-2A with synthetic DNAs carrying the respective mutations; some silent mutations were also introduced to generate restriction endonuclease sites used for identification of the plasmids constructed. The mutant plasmids differ from pRII-2A as follows (the substituted nucleotides with residue numbers[6] are given and the plasmids carrying mutated cDNAs are named after the mutant specification). pAM(R217Q): G, 648, 651, 699; A, 650; C, 696. pAM(R220Q): CAG, 658–660; C, 696; G, 699. pAM(R223Q): C, 667, 696; A, 668; G ,699. pAM(K226Q): C, 673, 676; G, 678. pAM(K226E): G, 676, 678, 699; C, 696. pAM(K226D): C, 673, 675; G, 676; T, 678. pAM(K226R): C, 672; A, 675; G, 677. pAM(S229R): G, 669; C, 672, 673; AGA, 685–687. pAM(R217Q·R220Q): G, 648, 651, 699; A, 650; CAG, 658–660; C, 696. pAM(R217Q·R223Q): G, 648, 651, 699; A, 650, 668; C, 667, 696. pAM(R217Q·K226Q): G, 648, 651, 678; A, 650; C, 673, 676. pAM(R220Q·R223Q): CAG, 658–660; C, 667, 696; A, 668; G, 699. pAM(R220Q·K226Q): CAG, 658–660; C, 673, 676; G, 678. pAM(R223Q·K226Q): C, 667, 676; A, 668; G, 678. pAM(K226R·S229R): C, 672; A, 675; G, 677; AGA, 685–687. pAM(S229K·P232R): C, 673, 693, 696; T, 675; G, 678, 695; AAA, 685–687. pAM(R217Q·R220Q·R223Q): G, 648, 651, 699; A, 650, 668; CAG, 658–660; C, 667, 696. pAM(R217Q·R220Q·K226Q): G, 648, 651, 678; A, 650; CAG, 658–660; C, 673, 676. pAM(K862Q): T, 2,583; C, 2,584. pAM(K859Q·K862Q): C, 2,575, 2,578, 2,584. pAM(K226Q·K859Q·K862Q): C, 673, 676, 2,575, 2,578, 2,584; G, 678. Deletion mutants were constructed by removing a cDNA segment from pRII-2A using restriction endonucleases, exonuclease III and/or mung bean nuclease. For the construction of pADI/II/III-2 and pADIV-2, synthetic oligonucleotides were also used to introduce a termination or an initiation codon. Sodium channel mutants derived from the individual plasmids or their combinations are as follows (the numbers of the amino-acid residues encoded and the additional C-terminal sequence resulting from the strategy used, if any, are given in parentheses): ΔN: pADN (1–13/50–2,005). cX-1: pADI-2 (1–632 plus HQGK) plus pADII/III/IV-2 (1–6/670–2,005). cX-2: pADI-1 (1–481 plus DQGK) plus pADII/III/IV-1 (1–6/583–2,005). cX-3: pADI-1 plus pADII/III/IV-2. cY-1: pADI/II-1 (1–1,144/2,000–2,005) plus pADIII/IV-1 (1–6/1,145–2,005). cY-2: pADI/II-2 (1–1,111 plus YQGK) plus pADIII/IV-2 (1–6/1,158–2,005). ΔY: pADY (1–1,022/1,121–2,005). cZ-1: pADI/II/III-1 (1–1,503/2,000–2,005) plus pADIV-1 (1–8/1,504–2,005). cZ-2: pADI/II/III-2 (1–1,504) plus pAD IV-2 (initiating methionine plus 1,506–2,005). ΔC: pADC (1–1,893 plus DQGK). All the constructs were confirmed by sequencing[30] the portions encompassing the synthetic DNA and ligation sites and by restriction endonuclease analysis.

pairs and the displacement of segment S4 within the transmembrane electric field may be the origin of the charge movement that accompanies the opening and closing of the sodium channel pore and confers voltage dependence on this gating process. If this is the case, replacement of a positively charged residue in segment S4 by a neutral or a negatively charged residue would be expected to alter the gating properties of the sodium channel. We investigated several mutants of this type in which mostly the S4 region of repeat I (Fig. 1*b*) was altered. Mutagenesis was focused on this region because it is the S4 segment which has the least number of positively charged residues and thus the largest effects of charge modifications would be anticipated. A few mutations in segment S4 of repeat II (Fig. 1*b*) were also included.

No appreciable expression of functional sodium channels in *Xenopus* oocytes was observed for any of the mutants that involved neutralization of more than three positive charges in segment S4 of repeat I and/or repeat II. All the single-, double- and triple-site mutations tested, however, yielded measurable expression of sodium channels. Mutations are indicated by the amino-acid residues (in one-letter code) in the wild-type and the mutant preceding and following the number[6] of the altered residue, respectively.

Figure 2*a* exemplifies current records for the wild-type sodium channel (1) and two mutants, K226Q (2) and R217Q·K226Q (3). The current records were fitted to m^3h kinetics using a least-squares method to yield time constants for activation (τ_m) and inactivation (τ_h); examples of least-squares fits are shown by the smooth lines superimposed on the responses to −20 mV (indicated by arrows). The non-linear voltage dependence of instantaneous currents, assessed by tail current analysis[22], was used to translate the apparent steady-state current in the absence of inactivation into an apparent asymptotic open-channel probability (m^3_∞). The voltage dependence of steady-state inactivation (h_∞) was obtained according to standard protocols[17]. Figures 2*b*, *c* and *d* show the voltage dependence of τ_m and τ_h, of peak currents and instantaneous tail currents and of m^3_∞ and h_∞, respectively, for the wild-type and the mutant K226Q.

The functional properties of the mutants studied are summarized in Table 1, which gives, among others, the potentials at which the HH parameters for activation and inactivation are half-maximal ($V^m_{1/2}$ and $V^h_{1/2}$), the valence of the apparent single-gate charge for activation (z_m) and the steepness of the potential dependence of inactivation (a_h). A decrease in z_m and thus a decrease in the slope of the relation of steady-state activation (m_∞) versus membrane potential is expected to result from a reduction in the net charge in those elements involved in the potential-dependent gating process. This is indeed the case for some mutant sodium channels, as exemplified in Fig. 3*a*. Replacement of one arginine or lysine residue in segment S4 of repeat I by a glutamine residue causes a significant reduction in z_m (R220Q, R223Q and K226Q), except for the mutation at position 217 (R217Q) (Table 1). However, double mutations combining R217Q with neutralization of positive charge at another site (R217Q·R220Q, R217Q·R223Q and R217Q·K226Q) intensify the effects of the latter mutations. The mutations K226E and K226D, which reduce the net positive charge at position 226 by two units, cause a stronger reduction in z_m than does the mutation K226Q. By contrast, the mutation K226R, which does not alter the positive charge at position 226, does not affect the z_m value. In Fig. 3*b*, the valence of the apparent single-gate charge, z_m, is plotted as a function of the decrease in the total

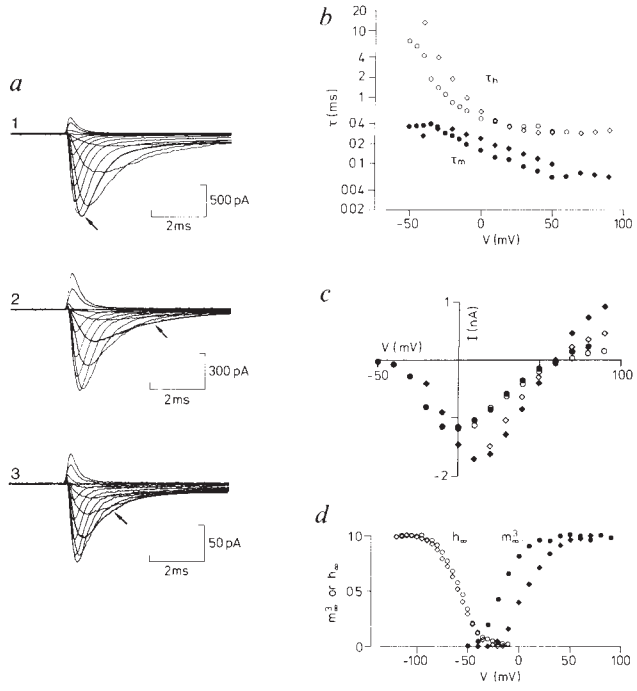

FIG. 2 *a*, Current responses to depolarizations in oocytes implanted with the wild-type (1) or with the mutant sodium channels K226Q (2) and R217Q·K226Q (3). *Xenopus* oocytes were injected with the wild type (0.20 μg μl^{-1}), K226Q (0.33 μg μl^{-1}) or R217Q·K226Q (0.33 μg μl^{-1}) mRNA. The responses were evoked by depolarizations ranging −60–+70 mV in 10-mV steps from a holding potential of −120 mV and they were recorded from cell-attached macro-patches[17,27]. Temperature: 15 °C. The data shown are the averages of 4 (1, 2) or 16 (3) individual traces. The current signals have been corrected for leakage and capacitive transients. Smooth lines superimposed on the −20-mV responses (arrows) show examples of least-squares fits according to HH-like kinetics as described below. *b*, Example of the voltage dependence of the time constants of activation (τ_m, filled symbols) and fast inactivation (τ_h, open symbols). Circles: wild-type; diamonds: K226Q. *c*, Example of the voltage dependence of peak currents (I_p, closed symbols) and instantaneous tail currents following a conditioning depolarization to +30 mV (I_t, open symbols). Circles: wild-type; diamonds: K226Q. *d*, Example of steady-state activation (m^3_∞, filled symbols) and inactivation (h_∞, open symbols) curves for wild-type (circles) and K226Q (diamonds) sodium channels.

METHODS. Records in *a* were fitted to m^3h kinetics plus a delay, δt, which decreased with depolarization and, for a holding potential of −120 mV, ranged from 0–110 μs (ref. 31). The fitting of each current response, $I(t)$, proceeded as follows. The decay phase of $I(t)$ was least-squares fitted with a double exponential function, $I_f(t)$, comprising a major fast component of inactivation with time constant τ_h and a slower component with a relative amplitude of less than 10% which is not further discussed. In a short interval around the peak, $I(t)$ was least-squares fitted with a third-order polynomial to obtain the best guess of the peak current, I_p, and of the time to the peak, t_p. The activation time constant, τ_m, and the delay, δt, were obtained from the least-squares fit during the rising phase of $I(t)/I_f(t)$ to the function $(1-\exp(-(t-\delta t)/\tau_m))^3$ up to 1.5 t_p. Assuming the same delay for m and h, $I_f(\delta t)$ was taken as the apparent steady-state current in the absence of inactivation, I'. Instantaneous tail currents, I_t, were obtained from separate protocols of stimulation comprising a fixed conditioning prepulse to +30 mV with duration $\sim t_p$ followed by a step to a variable tail potential. As discussed in ref. 22, division by I_t unfolds from I' the non-linear voltage dependence of the open-channel current, so that the asymptotic open-channel probability in the absence of inactivation, m^3_∞, was assumed to be proportional to the ratio I'/I_t. The latter quantity was least-squares fitted, assuming a voltage-dependence of m_∞ of the type:

$$m_\infty(V)=1\Big/\left(1+\exp\left(\frac{z_m e_0(V-V^m_{1/2})}{kT}\right)\right)$$

where e_0 is the electron charge (-1.60×10^{-19} coulomb), k is Boltzmann's constant and T is the absolute temperature. h_∞ plots were obtained from standard protocols[17] of voltage-clamp responses to test depolarizations eliciting maximal inward currents following 100 ms prepulses of variable amplitude. The data were least-squares fitted by a function of the type:

$$h_\infty(V)=1\Big/\left(1+\exp\left(\frac{V-V^h_{1/2}}{a_h}\right)\right)$$

number of net positive charges in segment S4 of repeat I. A roughly inverse relationship is observed between the z_m value and the decrease in total net positive charges. This finding provides experimental evidence that the positive charges in segment S4 of repeat I are directly involved in the voltage-sensing mechanism for activation. Although z_m is merely an empirical parameter whose absolute value is dictated by the use of the HH scheme, it should be stressed that the above effects are qualitatively model-independent because they are ultimately related to changes in the steepness of the voltage dependence of activation.

Extension of the S4 motif towards the C-terminus by substituting positively charged residues for neutral residues (S229R, K226R·S229R and S229K·P232R) does not increase the z_m value (Table 1). This suggests either that the side chains at positions 229 and 232 are not located within the membrane and are thus unable to sense the transmembrane field, or that they do not move along the field with gating. Neutralization of positive charges in segment S4 of repeat II at positions 859 and 862 exerts little effect on z_m (Table 1). No definite conclusion, however, can be drawn as to the role of segment S4 of repeat II because we have not systematically tested mutations of all the positively charged residues in this segment.

Some mutations that neutralize positive charges in segment S4 of repeat I cause shifts in the potential dependence of activation, as exemplified in Fig. 3*c*. In particular, the mutation K226Q, which involves neutralization of the last positive charge in segment S4 of repeat I, yields a positive shift of about 20 mV. Stronger charge modification at the same position (K226D and K226E) produces a comparable or an even larger shift in the same direction. A larger positive shift likewise results from neutralization of the positive charges at both positions 223 and 226 (R223Q·K226Q). Reduction of positive charges in segment S4 of repeat II, for example, K859Q·K862Q, also causes a positive shift. The effects of neutralizing positive charges in repeats I and II (K226Q·K859Q·K862Q) seem to be cumulative. On the other hand, some mutations, for example, R220Q and R217Q·R220Q, evoke a shift in the opposite direction. In general, neutralizations on the C-terminal side of segment S4 (positions 223 and 226) tend to cause a positive shift, whereas neutralizations on the N-terminal side (positions 217 and 220) tend to cause a negative shift. These shifts in $V^m_{1/2}$ could arise from modifications in the effective electric field experienced by the voltage-sensing structures. A positive shift is expected from neutralization of positive charges near the intracellular surface of the membrane, whereas a negative shift is expected from neutralization of positive charges near the extracellular surface[23]. Interpreting our results in terms of electrostatic effects

TABLE 1 Properties of wild-type and mutant sodium channels expressed in *Xenopus* oocytes

		Activation			Inactivation			
Mutant	ΔQ	$V^m_{1/2}$ (mV)	z_m (e_0)	*n*	$V^h_{1/2}$ (mV)	a_h (mV)	*n*	I_{mean} (pA)
Wild-type	0	−32±7	2.1±0.2	13	−61±9	10.4±1.3	9	704 (79-1,676)
R217Q	1	−34±7	2.1±0.3	6	−66±8	9.6±1.1	6	894 (200-1,573)
R220Q	1	−40±10	1.5±0.1	4	−67±21	9.9±0.8	4	461 (91-1,244)
R223Q	1	−20±9	1.6±0.2	5	−55±14	11.8±2.8	4	302 (99-644)
K226Q	1	−13±2	1.8±0.2	5	−67±6	11.3±1.0	5	1,373 (107-3,673)
K226E	2	−3±6	1.2±0.1	3	−71	9.9	2	470 (31-1,079)
K226D	2	−12±10	1.5±0.2	3	−69±14	10.4±2.2	3	226 (42-456)
K226R	0	−32±4	2.1±0.2	5	−70±7	10.4±1.7	4	543 (43-1,314)
S229R	−1 (0)	−25±3	2.1±0.2	3	−61±5	10.4±0.9	3	327 (120-462)
R217Q·R220Q	2	−51±5	1.2±0.2	5	−87±5	8.6±0.9	3	680 (166-1,634)
R217Q·R223Q	2	−49±2	1.3±0.1	4	−78±2	8.6±0.9	4	524 (372-665)
R217Q·K226Q	2	−14±10	1.5±0.1	4	−83±7	9.6±1.8	3	350 (100-501)
R220Q·R223Q	2	−28±16	1.6±0.2	4	—	—	—	153 (116-199)
R220Q·K226Q	2	−14±5	1.4±0.1	3	−61±3	10.8±2.8	3	349 (95-762)
R223Q·K226Q	2	−6±6	1.4±0.2	4	−70±14	12.4±1.2	3	209 (40-652)
K226R·S229R	−1 (0)	−25±4	2.0±0.1	4	−76±10	9.2±0.7	4	304 (92-403)
S229K·P232R	−2 (0)	−17±7	1.9±0.1	4	−63±8	9.9±1.2	4	610 (394-1,173)
R217Q·R220Q·R223Q	3	−44±13	1.2±0.2	3	−74	10.8	2	258 (108-385)
R217Q·R220Q·K226Q	3	−41±7	1.4±0.2	4	−82±12	13.1±3.4	3	342 (90-498)
K862Q	1 (0)	−22±5	2.1±0.1	5	−70±7	9.6±0.7	4	1,023 (456-1,903)
K859Q·K862Q	2 (0)	−5±7	2.1±0.2	6	−60±12	13.1±3.4	5	159 (20-339)
K226Q·K859Q·K862Q	3 (1)	11±9	1.8±0.3	5	−83±8	8.9±1.0	4	67 (25-170)
ΔN	0	−31±3	2.0±0.2	5	−68±11	13.8±1.5	5	130 (46-289)
cX-1	0	—	—	4	—	—	4	
cY-1	0	−46±7	2.0±0.3	3	−75±10	11.8±2.3	3	262 (66-900)
cY-2	0	−33±2	2.0±0.1	3	−78±5	13.1±1.4	3	333 (119-529)
ΔY	0	−31±3	2.2±0.2	5	−71±8	12.4±1.2	5	103 (66-141)
cZ-1	0	−36±6	2.2±0.2	4	−60±7	13.8±1.5	3	65 (37-105)
cZ-2	0	−37±4	1.8±0.1	3	−61	11.3	2	131 (86-158)
ΔC	0	−40±8	2.2±0.2	5	−80±9	8.3±1.1	3	180 (70-331)

Data are given as means ± s.d. for the wild-type sodium channel and the sodium channels with point mutations in segment S4 of repeats I and/or II (upper part) and for those with a deletion, a cut or a cut/addition (lower part). All the data are taken from cell-attached macro-patch recordings. ΔQ is the reduction in positive charge caused by the mutation; the values in parentheses are the reduction in positive charge at amino-acid positions 217, 220, 223 and 226 of segment S4 of repeat I. $V^m_{1/2}$ and $V^h_{1/2}$ are the single-gate equilibrium potentials of activation and inactivation. z_m, Valence of the apparent single-gate charge for activation; a_h, the slope factor, which is inversely proportional to the maximal derivative of the inactivation curve (see Fig. 2 legend); the average values for z_m and a_h are rounded to two digits. *n*, Number of oocytes used, taken from at least two different series of successful injections; several patches were obtained from most oocytes. I_{mean} is the mean peak sodium current observed; the range of peak currents is given in parentheses to show the variability in the level of expression from one batch of oocytes to another. No inactivation data are available for R220Q·R223Q. cX-1 yielded currents too small to allow reliable measurements. mRNAs specific for the wild-type and mutant sodium channels were synthesized *in vitro* using *Sal*I-cleaved plasmids as templates[16]. *Xenopus laevis* oocytes were injected[17] with the wild type (0.2 μg μl^{-1}) or a mutant mRNA (0.2–0.5 μg μl^{-1}; total concentration of an equimolar mixture for c-type mutants) and incubated[17] for 4–7 days. Measurements of macroscopic currents in cell-attached membrane patches were made as described previously[17,27].

is qualitatively consistent with current models of the orientation of segment S4 with respect to the membrane[5,6,24-26].

In addition to the purely electrostatic effects mentioned above, point mutations are expected to affect the equilibrium between different channel conformations by modifying interactions between amino-acid residues. A shift in the potential dependence of activation could be explained by assuming that only one of the voltage sensors is predominantly affected, either becoming a determinant of voltage-dependent activation (positive shift) or becoming fully activated in the potential range where the activation of the other sensors occurs (negative shift). It is interesting in this context that large shifts in $V^m_{1/2}$ in both directions are usually accompanied by strong reductions in z_m for sodium channels with mutations in segment S4 of repeat I (K226E, R217Q·R220Q and R217Q·R223Q). In the case of a positive shift, the voltage sensor affected dictates the potential sensitivity since the other sensors are already at least partially activated. Because this one voltage sensor carries only a fraction of the total gating charge, the slope of the potential dependence of activation would be reduced. In the case of a negative shift, the potential-dependent activation would be dictated by fewer voltage sensors, also giving a smaller apparent z_m. However, any simplistic molecular interpretation, based on three identical independent activation gates, should be taken with reservations.

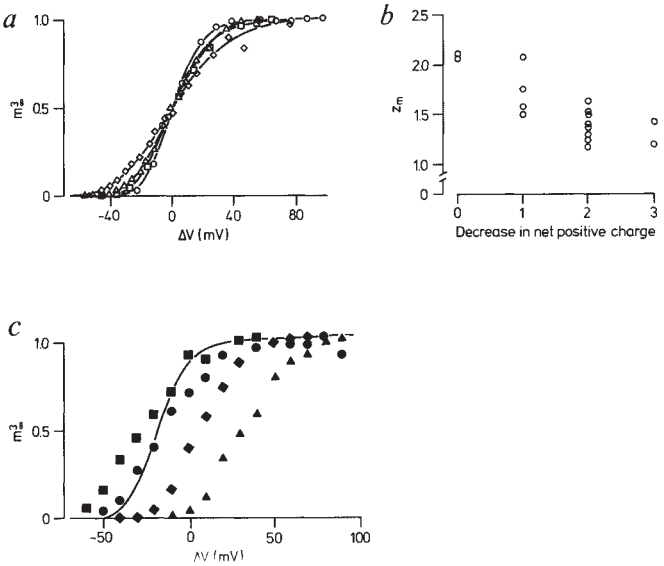

FIG. 3 *a*, Comparison of the steepness of the voltage dependence of steady-state activation (m^3_∞) for the wild-type (○) and the mutant sodium channels K226Q (□), R217Q·K226Q (△) and R217Q·R220Q·R223Q (◇). Single representative experiments are shown. For the purpose of making changes in slope readily visible, the activation curve of each mutant has intentionally been shifted along the voltage axis to have the same voltage of half activation as the wild-type. The continuous lines correspond to the best fits of the data points (see Fig. 2 legend). The valence of the apparent single-gate charge, z_m, is 2.1, 1.7, 1.5 and 1.1, respectively. These values represent the valence of the gating charge contributed by a single gate if a hypothetical channel comprising three identical gating subunits is assumed. *b*, Changes in z_m with decreases in the total number of net positive charges in segment S4 of repeat I at amino-acid positions 217, 220, 223 and 226. The values plotted as z_m are the average z_m values given in Table 1, but with one more digit to avoid overlapping of similar data points. Replacement of a positively charged residue by a negatively charged one is counted as a decrease of two net positive charges. *c*, Shifts of the voltage dependence of steady-state activation (m^3_∞) for mutant sodium channels. The continuous lines represent the best fit of the data for the wild-type sodium channel, assuming the following parameters for activation: a single-gate equilibrium potential (m_∞=0.5, $V^m_{1/2}$) of −32 mV and a z_m value of 2.1. Single representative experiments for the mutant sodium channels are shown and their $V^m_{1/2}$ (in mV) and z_m values are as follows: R217Q·R220Q (■), −53 and 1.2; R220Q (●), −38 and 1.4; K226Q (◆), −13 and 1.7; K226Q·K859Q·K862Q (▲), +10 and 1.6.

The potential dependence of the time constants of activation and inactivation for the wild-type and the mutant K226Q is shown in Fig. 2*b*. It is seen that for this mutant the voltage dependence of τ_m and τ_h shows a shift similar to that of $V^m_{1/2}$. The steady-state properties of inactivation are not systematically affected by the mutations in segment S4 of repeat I (Table 1 and Fig. 2*d*).

Expression of deletion mutants

The presence of four internal repeats suggests that the sodium channel evolved by duplications of an ancestral gene[5]. To examine whether individual repeats or their combinations can form functional sodium channels, we prepared mRNAs encoding single repeats or several contiguous repeats by transcription *in vitro* of the corresponding cDNAs (Fig. 1*c*). Δ-Type mutants were produced by injection into *Xenopus* oocytes of an mRNA encoding the sodium channel protein with a deletion. c-Type mutants were generated by injection of an equimolar mixture of two mRNAs encoding adjacent fragments of the sodium channel protein separated by a cut, either with an addition of four to eight residues at each end of the cut (cut/addition) or with substitution of the initiating methionine for the N-terminal residue of the C-terminal fragment (cut). mRNAs encoding only repeat I (derived from the plasmid pADI-1 or pADI-2; see Fig. 1 legend), repeat IV (pADIV-1 or pADIV-2), repeats I/II (pADI/II-1 or pADI/II-2), repeats III/IV (pADIII/IV-1 or pADIII/IV-2), repeats I/II/III (pADI/II/III-1 or pADI/II/III-2) or repeats II/III/IV (pADII/III/IV-1 or pADII/III/IV-2) did not give rise to sodium currents that could be measured using the two-electrode voltage clamp. Combinations of two mRNAs encoding repeat I and repeats II/III/IV (cX-1, cX-2 and cX-3 each having a cut/addition at different positions between repeats I and II; see Fig. 1*c* and legend) produced marginal sodium currents. By contrast, significant expression of sodium currents was observed for the mutants with a cut/addition (cY-1 and cY-2) or a deletion (ΔY) between repeats II and III, the mutants with a cut/addition (cZ-1) or a cut (cZ-2) between repeats III and IV and the mutants with a

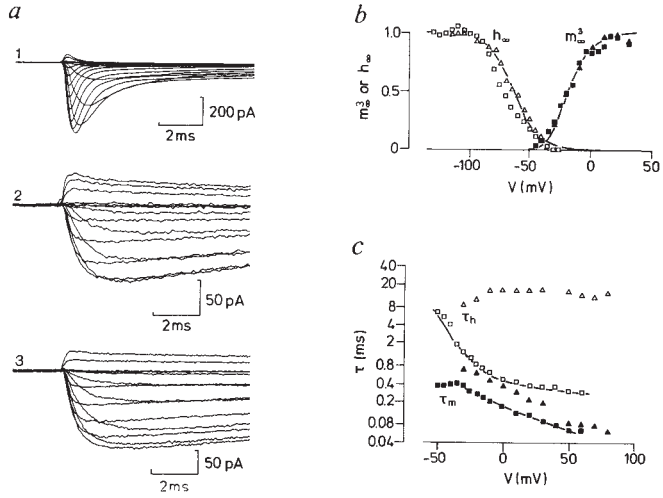

FIG. 4 *a*, Current responses to depolarizations in oocytes injected with the mutant sodium channel cY-2 (1) (0.33 μg μl^{-1}), cZ-1 (2) (0.33 μg μl^{-1}) or cZ-2 (3) (0.5 μg μl^{-1}) mRNA. Responses were evoked by depolarizations ranging −60–+70 mV (+90 mV for 1) in 10 mV steps from a holding potential of −120 mV. Averages of 16 individual traces. Temperature: 15 °C. *b*, Voltage dependence of steady-state activation (m^3_∞, filled symbols) and inactivation (h_∞, open symbols) for cY-2 (■, □) and for cZ-1 (▲, △). The smooth lines represent the best fit of the data for the wild-type in Fig. 2*d*. *c*, Voltage dependence of the time constants of activation (τ_m, filled symbols) and inactivation (τ_h, open symbols) for the same mutant channels as in *a* and *b*. The continuous lines correspond to the wild-type data in Fig. 2*b*.

deletion in the N-terminal (ΔN) or the C-terminal (ΔC) region. These results suggest that all four repeats are required for the formation of functional sodium channels.

Effects on inactivation

In Fig. 4*a*, macroscopic currents recorded from oocytes implanted with the mutant cY-2 (1), cZ-1 (2) or cZ-2 (3) are shown. Apart from their magnitude, the currents produced by the mutant cY-2, which has a cut/addition between repeats II and III, are similar to the wild-type (Fig. 2*a*, 1). By contrast, the currents evoked by the mutants cZ-1 and cZ-2, which have a cut/addition or a cut, respectively, between repeats III and IV, are characterized by a dramatic decrease in the rate of inactivation. A quantitative comparison of the steady-state and kinetic properties of cY-2 and cZ-1 with those of the wild-type channel is shown in Fig. 4*b*, *c*. For both mutants, the steady-state properties of activation and inactivation are similar to those of the wild-type. However, the τ_m of the mutant cZ-1 increases by a factor of about 1.8 and the τ_h of the mutant cZ-1 becomes nearly voltage-independent, being about 30-fold greater at strong depolarizations than that of the wild-type.

To characterize the properties of the mutant cZ-1 in greater detail, we measured the currents flowing through single channels, using smaller-diameter patch pipettes[17,27]. By contrast with the wild-type channel which exhibits short openings clustered at the beginning of the depolarization[17], openings sometimes lasted for periods as long as the voltage step (80 ms) (Fig. 5*a*). The open-time histogram for elementary currents flowing through the mutant cZ-1 channel is shown in Fig. 5*b*. The data are well fitted by a single exponential with a mean open time of 5.8 ms. Similar values were obtained over the potential range −60–+10 mV. By contrast, the mean open time of the wild-type channel measured at −32 mV is more than one order of magnitude smaller[17]. Single-channel current amplitudes measured for the cZ-1 channel in the potential range −40–+10 mV are plotted in Fig. 5*c*. The slope conductance of 15.7 pS (mean of two experiments) obtained for the cZ-1 channel is reasonably close to the value of 19 pS estimated for the wild-type channel[17].

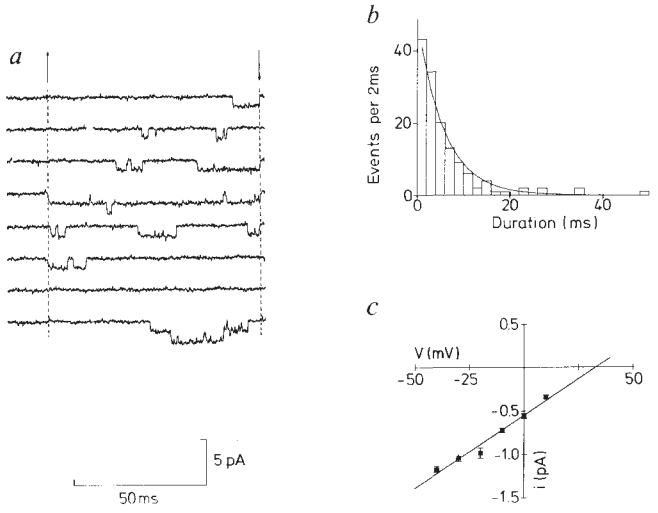

FIG. 5 *a*, Single-channel currents recorded from a patch on an oocyte implanted with the mutant sodium channel cZ-1. Responses to successive 80-ms depolarizations to −20 mV from a holding potential of −100 mV are shown. The dashed lines indicate the beginning and end of the pulse. The closed channel current level is the same as that before the start of the pulse. The original data were sampled at intervals of 50 μs and filtered at 4 kHz (−3 dB). Leakage subtraction was performed as follows. A fourth-degree polynomial was fitted to the current after the decline of the capacitive transients, for an average of eight hyperpolarizing pulses to −140 mV. The first few microseconds of the capacitive transients were left unchanged. This composite trace was then scaled and subtracted from each original trace. This method of leak subtraction introduces significantly less noise than conventional methods. Subsequently, the data were digitally filtered with a gaussian filter at 2 kHz (ref. 32). *b*, Distribution of open times from 140 single-channel events recorded at −20 mV. Openings shorter than 500 μs were disregarded. The distribution is fitted by a single exponential with a decay time constant of 5.8 ms, using a maximum likelihood method. *c*, Single-channel current-voltage relation. The straight line corresponds to a slope conductance of 17.3 pS.

The drastic slowing of the decay phase of macroscopic sodium currents and the increase in the mean open time of single-channel currents observed for the mutant cZ-1 are similar to the effects reported for native sodium channels treated with intracellularly applied endopeptidases[22,28,29]. We tested the action of trypsin on the sodium channel expressed in oocytes injected with the wild-type mRNA. In inside-out patches, a nearly complete removal of sodium current inactivation was observed after treatment with trypsin (50 μg ml^{-1}; for 10 min at 16 °C) (data not shown). An increase in peak sodium current was also seen after removal of inactivation, as described for the squid axon[22].

It has been proposed that the four internal repeats of the sodium channel, containing all putative transmembrane segments, are linked by three relatively large hydrophilic regions (53–326 amino acids in length in rat sodium channel II; see ref. 6). All these regions, together with the hydrophilic N- and C-terminal regions, are assigned to the cytoplasmic side of the membrane. Although cleaving the link between repeats III and IV affects mainly the rate of inactivation, the integrity of the link between repeats II and III seems to be of less functional importance. Neither cleaving the link between repeats II and III (cY-1 and cY-2), nor making a relatively large deletion in this region (ΔY) causes appreciable effects (Table 1). This is also the case for a deletion in the N-terminal (ΔN) or the C-terminal (ΔC) region (Table 1). These results indicate that the region between repeats III and IV is important for the inactivation of the sodium channel and that this region is likely to contain the sites at which intracellular proteolytic digestion exerts its effects. Because the mutants with a cut/addition in the region between repeats I and II fail to exhibit sodium currents large enough to allow detailed analysis, the possibility that this region is also involved in inactivation cannot be excluded. Our results are consistent with the proposed intracellular location of the region between repeats III and IV. This region contains a cluster of conserved positively charged residues (mainly lysine) and has been proposed to be involved in the inactivation of the sodium channel[6].

Discussion

Functional analysis of mutated sodium channels expressed in *Xenopus* oocytes allows us to gain several types of information about the structure-function relationship of this voltage-gated ionic channel. Our results show that reducing the net positive charge in segment S4 of repeat I causes a decrease in the apparent gating charge, as manifested by a reduction in the steepness of the potential dependence of activation. This finding provides experimental evidence that the positive charges in segment S4 of repeat I constitutes at least part of the gating charge involved in the voltage-dependent activation of the sodium channel. The unique structural features of segment S4 are strikingly well conserved in the calcium channel[9,10] and the potassium channel[11–15], which show amino-acid sequence homology with the sodium channel. This implies that the involvement of the clustered positive charges in segment S4 represents a common mechanism responsible for the activation of voltage-gated ionic channels.

Our results also show that cleavage of the linkage between repeats III and IV of the sodium channel causes a strong reduction in the rate of inactivation. This finding, together with the similar effect observed for the wild-type sodium channel treated with intracellularly applied endopeptidases, supports the view that this region, located on the cytoplasmic side of the

membrane, is involved in the inactivation of the sodium channel.

Another finding of the present investigation is that the homologous internal repeats of the sodium channel can function as structural units to form functional channels, even when a linkage between the repeats is cleaved. However, unlike the potassium channel which has a basic structure corresponding to a single repeat of the sodium channel[11,13-15] and is assumed to form a homo-oligomeric complex[12], all four repeated units are required for the formation of functional sodium channels. This suggests that, during the evolution of the sodium channel by gene duplications, each of the four repeated units may have acquired a differentiated function. □

Note added in proof: Since the submission of the first version of this manuscript, it has been reported that antibody directed against a peptide sequence in the region between repeats III and IV slows inactivation of the sodium channels[33].

Received 28 March; accepted 28 April 1989.

1. Hodgkin, A. L. & Huxley, A. F. *J. Physiol., Lond.* **117,** 500–544 (1952).
2. Hille, B. *Ionic Channels of Excitable Membranes* (Sinauer, Sunderland, Massachusetts, 1984).
3. Armstrong, C. M. & Bezanilla, F. *Nature* **242,** 459–461 (1973).
4. Keynes, R. D. & Rojas, E. *J. Physiol., Lond.* **239,** 393–434 (1974).
5. Noda, M. *et al. Nature* **312,** 121–127 (1984).
6. Noda, M. *et al. Nature* **320,** 188–192 (1986).
7. Kayano, T., Noda, M., Flockerzi, V., Takahashi, H. & Numa, S. *FEBS Lett.* **228,** 187–194 (1988).
8. Salkoff, L. *et al. Science* **237,** 744–749 (1987).
9. Tanabe, T. *et al. Nature* **328,** 313–318 (1987).
10. Tanabe, T., Beam, K. G., Powel, J. A. & Numa, S. *Nature* **336,** 134–139 (1988).
11. Tempel, B. L., Papazian, D. M., Schwarz, T. L. Jan, Y. N. & Jan, L. Y. *Science* **237,** 770–775 (1987).
12. Timpe, L. C. *et al. Nature* **331,** 143–145 (1988).
13. Pongs, O. *et al. EMBO J.* **7,** 1087–1096 (1988).
14. Tempel, B. L., Jan, Y. N. & Jan, L. Y. *Nature* **332,** 837–839 (1988).
15. Baumann, A., Grupe, A., Ackermann, A. & Pongs, O. *EMBO J.* **7,** 2457–2463 (1988).
16. Noda, M. *et al. Nature* **322,** 826–828 (1986).
17. Stühmer, W., Methfessel, C., Sakmann, B., Noda, M. & Numa, S. *Eur. biophys. J.* **14,** 131–138 (1987).
18. Suzuki, H. *et al. FEBS Lett.* **228,** 195–200 (1988).
19. Auld, V. J. *et al. Neuron* **1,** 449–461 (1988).
20. Armstrong, C. M. & Bezanilla, F. *J. gen. Physiol.* **70,** 567–590 (1977).
21. Aldrich, R. W., Corey, D. P. & Stevens, C. F. *Nature* **306,** 436–441 (1983).
22. Stimers, J. R., Bezanilla, F. & Taylor, R. E. *J. gen. Physiol.* **85,** 65–82 (1985).
23. Hille, B., Woodhull, A. M. & Shapiro, B. I. *Phil. Trans. R. Soc. Lond. B* **270,** 301–318 (1975).
24. Guy, H. R. & Seetharamulu, P. *Proc. natn. Acad. Sci. U.S.A.* **83,** 508–512 (1986).
25. Greenblatt, R. E., Blatt, Y. & Montal, M. *FEBS Lett.* **193,** 125–134 (1985).
26. Caterall, W. A. *A. Rev. Biochem.* **55,** 953–985 (1986).
27. Methfessel, C. *et al. Pflügers Arch.* **407,** 577–588 (1986).
28. Rojas, E. & Armstrong, C. M. *Nature new Biol.* **229,** 177–178 (1971).
29. Armstrong, C. M., Bezanilla, F. & Rojas, E. *J. gen. Physiol.* **62,** 375–391 (1973).
30. Sanger, F., Nicklen, S. & Coulson, A. R. *Proc. natn. Acad. Sci. U.S.A.* **74,** 5463–5467 (1977).
31. Keynes, R. D. & Rojas, E. *J. Physiol., Lond.* **255,** 157–189 (1976).
32. Colquhoun, D. & Sigworth, F. J. in *Single-Channel Recording* (eds Sakmann, B. & Neher, E.) 191–263 (Plenum, New York, 1983).
33. Vassilev, P. M., Scheuer, T. & Catterall, W. A. *Science* **241,** 1658–1661 (1988).

ACKNOWLEDGEMENTS. We thank Drs F. Ashcroft, M. B. Jackson and G. Augustine for reading the manuscript and M. Push for help with the single-channel analysis. This investigation was supported in part by the Ministry of Education, Science and Culture and the Science and Technology Agency of Japan, the Mitsubishi Foundation and the Japanese Foundation of Metabolism and Diseases.

Intense 6.7-keV iron line emission from the Galactic Centre

K. Koyama*, H. Awaki*, H. Kunieda*, S. Takano*, Y. Tawara*, S. Yamauchi*, I. Hatsukade† & F. Nagase‡

* Department of Astrophysics, Nagoya University, Furo-cho, Chikusa-ku, Nagoya 464, Japan
† Department of Physics, Osaka University, Toyonaka, Osaka 565, Japan
‡ Institute of Space and Astronautical Science, 3-1-1 Yoshinodai, Sagamihara, Kanagawa 229, Japan

THE Galactic Centre, although obscured by dust at optical wavelengths, is luminous in higher-energy radiation. Gamma-ray observations suggest that a large number of supernovae or novae, or a single supermassive object, has exploded in the Galactic Centre[1]. Such an explosion will heat up the interstellar medium, probably creating an optically thin hot plasma. Here we report the discovery of intense iron-line emission at 6.7 keV from the Galactic Centre, detected by the Ginga satellite, with characteristics consistent with its production by a shock-heated plasma. The line intensity peaks at the Galactic Centre with a surface brightness of $\sim 1.5 \times 10^{-7}$ erg s^{-1} sr^{-1} cm^{-2} and extends over an angular size of 1.8°. The total luminosity of the iron line at the centre region is $\sim 2.1 \times 10^{36}$ erg s^{-1} assuming that the distance to the centre is 10 kpc. The line intensity at the centre is about ten times larger than that from the region of the galactic ridge. The line feature observed is consistent with thermal emission from a thin hot plasma at a temperature of ~10 keV. The abundance of iron is estimated to be comparable to or larger than the cosmic abundance. This thin hot plasma is attributable to a shock-heated interstellar medium by an energetic explosion.

In the X-ray continuum energy band, several point sources and unresolved diffuse emission have been discovered in the Galactic Centre region. (See, for example, refs 2–4 and references therein). However, the continuum X-ray intensity in the region of the Galactic Centre is not particularly strong compared with that in the other regions of the Galaxy, in contrast to radio, infrared and γ-ray bands. An optically thin hot plasma can produce characteristic X-rays from highly ionized atoms. Thus, observations of characteristic X-rays may provide a new clue to activity near the Galactic Centre, and we therefore carried out X-ray mapping of iron K-line emission along the galactic plane.

The galactic plane was scanned with the large-area proportional counters (LAC)[5] on board the X-ray astronomy satellite Ginga[6] on several occasions: August and October in 1987 and March in 1988. The total effective area of the LAC is 4,000 cm^2, with a field of view (or beam size, full width at half maximum) of 1° along and 2° perpendicular to the scan path. Apart from point sources, we see no time variability of X-ray flux during these three scans, and these scan data, within 0.5 ° of the plane, were superposed to construct the X-ray profile along the galactic longitude. In Fig. 1*a*, we show the X-ray intensity profile on the galactic plane in the continuum energy band 2–18 keV. We see many prominent peaks corresponding to known binary X-ray sources (but no prominent peaks are seen at the Galactic Centre.

We then sliced the scan data and constructed the X-ray spectrum for each position on the galactic plane (to 0.4° resolution). Figure 2 shows the spectrum near the Galactic Centre. An intense emission-line feature at 6.7 keV is observed, as was already noted by Koyama[7]. In order to evaluate the line energy and intensity from the galactic plane, we fitted a model assuming a free–free spectrum for the continuum and a narrow emission line. Most of the data, except for the data near bright X-ray binary sources, can be fitted with this model. Using the acceptable results, we plotted the best-fit intensity and energy of the emission line against galactic longitude, as shown Fig. 1*b*, *c*. A remarkable feature discovered here is a strong peak in line intensity near the Galactic Centre. Here, the line intensity is stronger than those from the bright point sources (the average intensity of the iron line at the peaks of the six brightest sources is ~70% of that of the Galactic Centre), although they are not shown because of large statistical errors resulting from strong continuum intensities. The broad hump near galactic longitude $l = 30°$ corresponds to the '5 kpc ring' where the CO-line and infrared and γ-ray intensities show local maxima[8]. The peak at $l = 25°$ and complex structure near $l = 350°$ are due to point sources. The energy of the emission line is consistent with 6.7 keV, suggesting that it corresponds to the K-line of helium-